Transmission Electron Microscopy Studies of Bufferless Epitaxial GeSn on (0001) Sapphire

Jiechao Jiang, Nonso Martin Chetuya, Joseph H Ngai, Gordon J. Grzybowski, and Efstathios I. Meletis

(Invited Paper)

***Abstract*—Epitaxial growth of GeSn films directly on (0001) sapphire substrates, has not been considered as a feasible task. Here, an ultra-thin and a 1 μm thick $Ge_{1-x}Sn_x$ ($x \leq 0.1$) film were deposited on (0001) sapphire substrates at 475 °C and 367 °C, respectively, through remote plasma-enhanced chemical vapor deposition (RPECVD). The ultra-thin $Ge_{1-x}Sn_x$ film (deposited at 475 °C) exhibits a distinct epitaxial/twin mushroom-like island morphology with a height ranging from 30-45 nm and a lateral width ranging from 40 - 200 nm. The $Ge_{1-x}Sn_x$ islands are covered by a ∼4 nm thick surface layer of Sn-rich amorphous material and present an atomically sharp and robust interface with the substrate. The epitaxial $Ge_{1-x}Sn_x$ lattices coherently join with the Al layer of the sapphire substrate. The 1 μm thick $Ge_{1-x}Sn_x$ film (deposited at 367 °C) consists of a thin epitaxial/twin layer below a nanocrystalline columnar layer. The nanocrystalline grains have varying Sn content that exceeds that in the epitaxial structure. The epitaxial/twin layer in this film has an ∼1 nm thick highly disrupted near amorphous layer at the interface. Quasiperiodic, two-dimensional hexagonal networks of misfit dislocations are formed at the interfaces of both films to accommodate the misfit strain. The dislocation periodic length was 13.3 Å and 13.1 Å for the films deposited at 475 °C and 367 °C, respectively. The epitaxial structures in both films have an identical orientation relationship of $(111)_{GeSn}//(0001)_{Sapphire}$, $[1\bar{1}0]_{GeSn}//[2\bar{1}\bar{1}0]_{Sapphire}$, $[21\bar{1}]_{GeSn}//[1\bar{1}00]_{Sapphire}$ with the substrate, exhibiting lattice mismatches of ∼15% between the (220) GeSn and the $(11\bar{2}0)$ Al_2O_3 along the interface plane and -24% between the (111) GeSn and the (0003) Al_2O_3 planes along the film growth direction. The observed microstructures provide valuable feedback that can be used to optimize the RPECVD process for better quality epitaxial GeSn on (0001) sapphire substrates with no buffer layer required.**

***Index Terms*—Diffraction, electron microscopy, interface phenomena, semiconductor epitaxial layers, thin films.**

Received 2 August 2024; revised 30 August 2024; accepted 2 September 2024. Date of publication 5 September 2024; date of current version 11 October 2024. This work was supported in part by the U.S. Air Force under Award FA8650-20-2-5853 and under subaward SPC-1000006781 | GR128665, and in part by the U.S. National Science Foundation Partnership for Research and Education in Functional Materials under Award NSF/DMR 2122128 and Award 2425164. *(Corresponding author: Jiechao Jiang.)*

Jiechao Jiang, Nonso Martin Chetuya, and Efstathios I. Meletis are with the Materials Science and Engineering Department, University of Texas at Arlington, Arlington, TX 76019 USA (e-mail: jiangjc@uta.edu; nonso.chetuya@mavs.uta.edu; meletis@uta.edu).

Joseph H Ngai is with the Department of Physics, University of Texas at Arlington, Arlington, TX 76019 USA (e-mail: jngai@uta.edu).

Gordon J. Grzybowski is with KBR, Beavercreek, OH 45431 USA (e-mail: gordon.grzybowski.ctr@us.af.mil).

Color versions of one or more figures in this article are available at https://doi.org/10.1109/JSTQE.2024.3454954.

Digital Object Identifier 10.1109/JSTQE.2024.3454954

I. Introduction

SAPPHIRE (Al_2O_3) exhibits a high melting point of 2030 °C, an excellent thermal conductivity of 42.5 W/(m·K), a relatively low thermal expansion coefficient of around 5.8×10^{-6} /°C and good resistance to thermal shock. It is transparent in the infrared region of the electromagnetic spectrum and maintains its physical and optical properties at high temperatures [1]. These favorable properties, in conjunction with its hardness, electrical insulating properties and other characteristics, make it a valuable material in various electronic, optical, aerospace, and high-temperature applications. Sapphire can be considered as one of the best insulator substrates for electronics and optoelectronics devices [2]. The significance of sapphire substrates has been growing in the field of electronics through the integration of semiconducting materials like ZnTe [2], Ge [3], [4], SiGe [5], [6], [7], [8], [9], [10], CdTe [11], and GaAs [12], [13] for various applications.

High-quality epitaxial $Ge_{1-x}Sn_x$ films with Sn content exceeding 6 at.%, offer promising electrical and optical properties pivotal for applications spanning near- and mid-infrared detectors, emitters, and lasers [14], [15], [16], [17], [18], [19], [20]. The motivation for this work, involving the growth and study of $Ge_{1-x}Sn_x$ films on sapphire substrates, is grounded in their potential applications in electronics, photonics, and optoelectronics. However, several obstacles, including: (a) the low bulk solubility of Sn in Ge, which is approximately 1 at.% [21], coupled with the propensity for Sn to segregate or precipitate from $Ge_{1-x}Sn_x$; (b) distinctly different crystal structures for GeSn (diamond cubic) and sapphire (Al_2O_3, hexagonal); and (c) the substantial lattice mismatch between $Ge_{1-x}Sn_x$ films and (0001) sapphire substrates, present considerable challenges in achieving high quality epitaxial $Ge_{1-x}Sn_x$ films. Recently, various innovative techniques using low-temperature, non-equilibrium growth processes have been developed to produce higher Sn content $Ge_{1-x}Sn_x$ films. One example among these methods is remote plasma-enhanced chemical vapor deposition (RPECVD) that provides the capability for fast growth of epitaxial GeSn films [22], [23].

Substantial lattice mismatches at the interface between the film and substrate introduce considerable tensile or compressive stress, resulting in microstructures enriched with defects and pose a significant hurdle to realizing high-quality films. To address this challenge, common approaches involve introducing

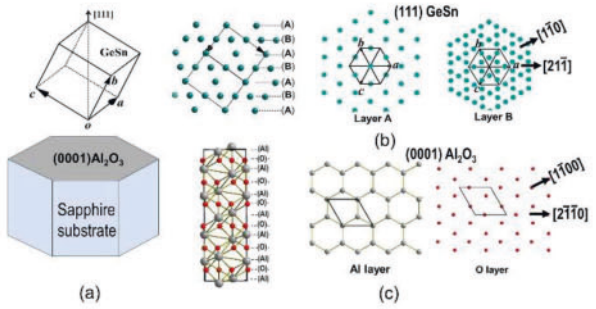

Fig. 1. (a) Illustration of possible epitaxial growth of GeSn on (0001) sapphire substrate; (b) schematic packing sequences of the A and B layers in GeSn along the [111] axis, and their atom arrangements in each layer; (c) schematic packing sequences of the Al and O layers and the corresponding atom arrangements.

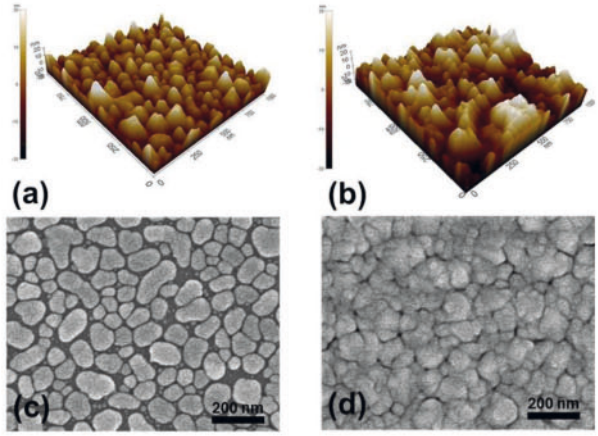

Fig. 2. (a) and (b) AFM, (c) and (d) SEM images of the $Ge_{1-x}Sn_x$ uHTIL and LTTF films, respectively.

an intermediate buffer layer or a graded buffer layer onto the substrate before film growth. These buffers aim to mitigate the strain and enhance film quality by minimizing the formation of defects [24], [25], [26], [27], [28]. Very recently, the first attempt to grow epitaxial $Ge_{1-x}Sn_x$ on a (0001) sapphire substrate using molecular beam epitaxy has been reported [29]. This epitaxial growth was accomplished by depositing a $Ge_{1-x}Sn_x$ film on engineered buffered Ge(111)/AlAs/Al_2O_3 (0001) substrates at 150 °C. In the present study, we present a comprehensive examination of the film and interface structures of two GeSn films grown directly on (0001) sapphire substrates by RPECVD. An ultra-thin film was used to understand and optimize the initial nucleation at the substrate interface and a thicker layer was prepared to evaluate how the film evolves. These growths were performed at different temperatures to optimize the crystallinity of the layers while preventing phase segregation. The objective of this study is to investigate the feasibility of epitaxially growing GeSn on a substrate with a markedly different crystal structure, a task that previously was not considered feasible. Characterization of the film and interface structure, along with the associated growth mechanism, can provide valuable insights for refining growth conditions, enhancing film quality, and contributing to the production of significantly higher-quality films.

II. Geometric Configuration of GeSn on (0001) Sapphire Substrate

Sapphire (Al_2O_3) exhibits a hexagonal crystal structure with unit cell lattice constants a = 4.765 Å and c = 12.991 Å, whereas GeSn has a diamond crystal structure [30]. For GeSn epitaxially grown on (0001) sapphire substrate, the most probable geometric configuration is the GeSn (111) plane grown on the (0001) plane of sapphire, as shown in Fig. 1(a). The crystal structure of GeSn can be obtained by alternately stacking atomic layers A and B, as shown in Fig. 1(b), along its [111] axis. The hexagons within the layers A and B contain 4 and 12 atoms, respectively. The dimension of the hexagons varies with the Sn content in the structure. In the sapphire crystal structure, Al^{3+} are surrounded by six O^{2-} forming an octahedral arrangement which results in a hexagonal close-packed structure by alternately stacking Al and O layers along the [0001] axis, Fig. 1(c). The terminating surface layer on the (0001) sapphire substrate can contain either Al or O atoms, as shown in Fig. 1(c). When a GeSn structure grows on a (0001) sapphire substrate, the first layer can be either A or B layer, and the two structures can possibly follow a crystallographic orientation relationship of $(111)_{GeSn}//(0001)_{Sapphire}$, $[1\bar{1}0]_{GeSn}//[2\bar{1}\bar{1}0]_{Sapphire}$, $[21\bar{1}]_{GeSn}//[1\bar{1}00]_{Sapphire}$.

III. Film Fabrication and Characterization

Two distinct films were deposited on (0001) sapphire substrates, an ultra-thin $Ge_{1-x}Sn_x$ ($x \leq 0.1$) initiation layer grown at a higher temperature of 475 °C (denoted as uHTIL) and a thicker ($\sim 1\ \mu$m) film grown at a lower temperature of 367 °C (denoted as LTTF). Ultrahigh purity, semiconductor grade (99.999%) GeH_4 and $SnCl_4$ chemical precursors were used for deposition. For substrate preparation, the (0001) sapphire substrates received a 10 minute anneal in an ozone cleaner prior to being introduced into the growth apparatus. During growth, a constant substrate temperature was maintained by feedback from a Eurotherm controller, measured by a thermocouple embedded in the substrate heater unit. The substrate temperature was determined based on separate calibration measurements made using a commercial thermocouple wafer and an optical pyrometer. The correlation between the heater thermocouple and wafer temperature was linear over the entire operating range. Further details of the growth process and deposition equipment have been previously reported [22], [23].

X-ray photoelectron spectroscopy (XPS) was conducted in a Perkin-Elmer Phi 560 ESCA/SAM system using Al K_α excitation (1484.6 eV), to investigate surface composition of the films. High resolution Ge 2p spectra, spanning the range of 1280-1200 eV, and Sn 3d spectra, ranging from 525-460 eV, were acquired with a 0.2 eV step size and a pass energy of 100 eV. Calibration of binding energy (BE) relied on the C 1s peak, positioned at 284.8 eV. Raman spectra were captured using a ThermoFisher DXR3 Raman microscope with a 532 nm laser. Atomic force microscopy (AFM) was conducted using a Park XE 70 AFM, while scanning electron microscopy (SEM) was carried out using a Hitachi S-4800 field-emission

microscope equipped with an EDAX energy dispersive spectroscopy (EDS) system, operating at 3 keV, to evaluate surface morphology.

X-ray diffraction (XRD) θ-2θ scans were obtained using a Bruker D8 Advance diffractometer using Cu K_α radiation. Cross-section (X-) and plan-view specimens were prepared for transmission electron microscopy (TEM) through mechanical grinding, polishing, and dimpling using a Gatan Model 656 dimple grinder. Subsequent Ar-ion milling was performed in a Gatan Model 691 precision ion polishing system (PIPS). The intricate microstructure of the films was examined in depth using a Hitachi H-9500 high-resolution (HR) transmission electron microscope operating at 300 keV. The microscope, with a lattice resolution of 0.10 nm, is equipped with an EDAX EDS system. HRTEM image simulations were performed using the EMS software [31].

IV. Results and Discussion

A. AFM, SEM, XPS, Raman and XRD Analysis

We have investigated the surface morphology and roughness of the $Ge_{1-x}Sn_x$ uHTIL and LTTF films using AFM and SEM with a scanning size area of $1 \times 1\ \mu m^2$. AFM images show rough island structures for both films, Fig. 2(a) and (b). The uHTIL and LTTF films exhibit average mean roughness (R_a) values of 5.19 nm and 6.88 nm, respectively. SEM images indicate that the surfaces of both films present a grainy morphology, Fig. 2(c) and (d). The grains in the uHTIL film are disjointed, with distinct dark wide boundaries between them, whereas the separations between islands in the LTTF film are more compact. The grain size varies from 30 - 150 nm in both films.

The Ge and Sn content on the surfaces of the two films was examined using XPS, Fig. 3(a). The average Sn content in the $Ge_{1-x}Sn_x$ uHTIL and LTTF films is ~34.1 at.% and ~8.6 at.%, respectively. The notable difference in Sn content between the two films was clear through the intensity variation of the Ge 2p and Sn 3d peaks in Fig. 3(b) and (c). The spectra of the Ge 2p and Sn 3d peaks from both films, as shown in Fig. 3(b) and (c), were acquired under identical conditions. The Ge 2p peak in the LTTF film exhibits significantly higher intensity compared to that in the UHTIL film, while the Sn 3d peak in the former is notably lower than in the latter. The Raman spectra of the $Ge_{1-x}Sn_x$ uHTIL and LTTF films exhibit peaks at 295.9 and 294.1 cm^{-1}, respectively (Fig. 3(d)). The Sn content estimated from the Ge–Ge vibration mode peak position is ~6.9% for the uHTIL and ~9% for the LTTF film, using the compositional dependence of the Ge–Ge mode position in GeSn alloys reported in the literature [32]. The peak observed at ~417 cm^{-1} in the $Ge_{1-x}Sn_x$ uHTIL spectrum corresponds to a phonon mode of Al_2O_3 [33]. The discrepancy between the estimate of 34.1% Sn derived from the XPS of the $Ge_{1-x}Sn_x$ uHTIL film and its notable difference derived from the Raman study will be discussed in more detail in the TEM section.

We have studied the $Ge_{1-x}Sn_x$ uHTIL and LTTF films on (0001) sapphire, and the bare substrate for comparison, using θ-2θ XRD analysis, as shown in Fig. 3(e). Only the (111) peak of the $Ge_{1-x}Sn_x$ uHTIL film on (0001) sapphire substrate was

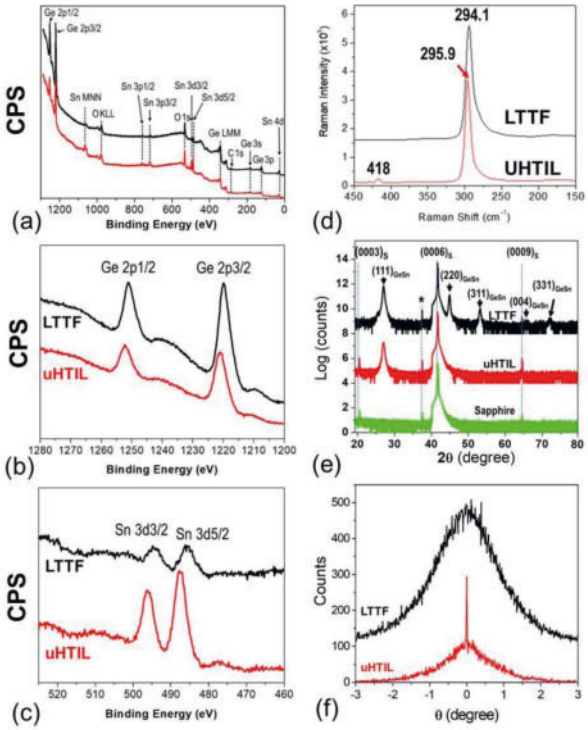

Fig. 3. (a) XPS survey spectra, (b) and (c) XPS high resolution spectra of Ge 2p and Sn 3d, (d) Raman spectra, (e) XRD spectra, (f) (111) GeSn rocking curves of $Ge_{1-x}Sn_x$ uHTIL and LTTF films on (0001) DSP sapphire substrates. Subscript "s" in (e) indicates substrate.

observed (center spectrum in Fig. 3(e)), indicating that the film is highly [111] axis oriented. The strong peaks at 27.07° and 41.70° with a d-spacing of 3.292 Å and 2.165Å, respectively, correspond to (111) GeSn and (0006) Al_2O_3. The lattice constant of the $Ge_{1-x}Sn_x$ epitaxial structure along the growth direction is 5.702 Å with a Sn concentration of 5.6 at.%. The XRD spectrum of the $Ge_{1-x}Sn_x$ LTTF (top spectrum in Fig. 3(e)) shows a strong peak at 27.09°, and weak peaks at 44.96°, 53.18°, 65.31° and 72.13° corresponding to d-spacings of 3.288 Å, 2.015 Å, 1.72 Å, 1.43 Å, and 1.31 Å, which can be determined to be the (111), (220), (311), (400), and (331) with lattice constants of 5.695 Å, 5.698 Å, 5.704 Å, 5.720 Å, and 5.710 Å, and Sn at.% of 4.7%, 5.1%, 5.8%, 7.8% and 6.6%, receptively. The weak peak marked by "$*$" corresponds to (0006) Al_2O_3 excited by residual Cu K_β. The presence of the strong (111) GeSn peak in LTTF indicates formation of an epitaxial GeSn structure with (111) orientation preferred in the film. The presence of the weak peaks indicates formation of GeSn nanocrystalline with different Sn content within this film. Fig. 3(f) provides rocking curves of the (111) GeSn in both films. The rocking curve from the $Ge_{1-x}Sn_x$ uHTIL exhibits a very sharp peak with a full width at half maximum (FWHM) of 0.1° atop a broad peak with an FWHM of 1°, indicating high epitaxial quality of the film. The rocking curve from the $Ge_{1-x}Sn_x$ LTTF on (0001) sapphire substrate shows a broad peak with an FWHM of 2°, indicating the presence of an epitaxial structure in the film. The microstructure of both films is examined in detail in the TEM studies below.

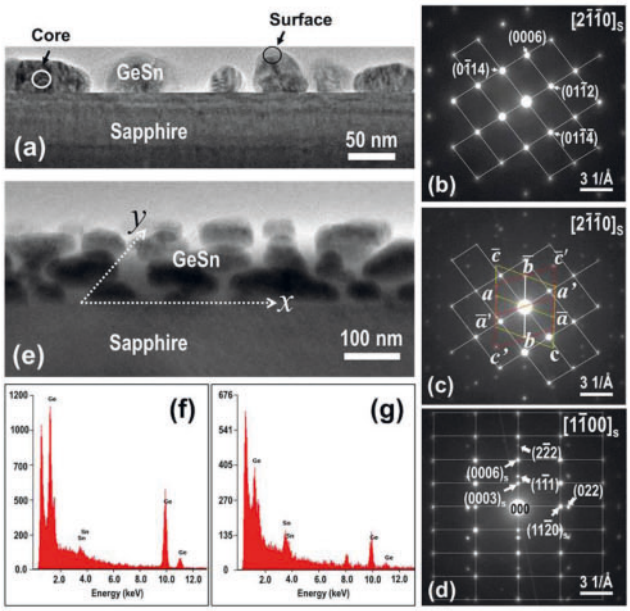

Fig. 4. (a) XTEM image of $Ge_{1-x}Sn_x$ uHTIL on (0001) sapphire substrate. (b) and (c) SAED patterns from sapphire substrate and GeSn/sapphire interface, respectively, along the $[2\bar{1}\bar{1}0]Al_2O_3$ direction. (d) SAED pattern of the GeSn/sapphire interface along the $[1\bar{1}00]$ Al_2O_3 direction. (e) XTEM image from a thick TEM foil of GeSn uHTIL on (0001) sapphire viewed along a direction tilted 10° away from the $[2\bar{1}\bar{1}0]$ Al_2O_3 direction. (f) and (g) EDS spectra from the core and the near-surface regions as depicted in (a), respectively. Subscript "s" indicates substrate.

B. TEM Studies of $Ge_{1-x}Sn_x$ uHTIL on (0001) Sapphire Substrate

Fig. 4(a) shows a cross-section TEM (XTEM) image of the $Ge_{1-x}Sn_x$ uHTIL on (0001) sapphire taken along the $[2\bar{1}\bar{1}0]$ Al_2O_3 direction, clearly revealing a discrete island-like morphology within the film. The islands exhibit a height ranging from 30-45 nm, a lateral width ranging from 40 - 200 nm, with distances between islands (the thickness of the boundaries between them) ranging from 4 nm to 70 nm. Selected Area Electron Diffraction (SAED) studies show that the distinct islands possess the same crystallographic orientation. Fig. 4(b) and (c) exhibit SAED patterns taken from the sapphire substrate, and multiple islands within the $Ge_{1-x}Sn_x$ uHTIL and the sapphire substrate along the $[2\bar{1}\bar{1}0]$ axis of Al_2O_3, respectively. The SAED pattern in Fig. 4(c) exhibits a clear superposition of the $[2\bar{1}\bar{1}0]$ Al_2O_3 (spots on the dashed lattice points, i.e., Fig. 4(b)) and the [110] GeSn diffraction patterns (spots marked by a ($\bar{a}$), b ($\bar{b}$), c ($\bar{c}$), a' ($\bar{a}'$) and c' ($\bar{c}'$)). Assuming that the diffraction spots labeled as a, b and c with indices $(\bar{1}1\bar{1})$, $(1\bar{1}\bar{1})$ and $(2\bar{2}0)$, respectively, belong to a [110] zone in GeSn, then spots a' ($\bar{a}'$), b ($\bar{b}$) and c' ($\bar{c}'$) belong to another [110] zone within a GeSn twin structure [34], [35]. The SAED study shows that GeSn epitaxial structure with some embedded twin structures is formed in the uHTIL film on (0001) sapphire substrate. The epitaxial structure of GeSn and the substrate have an orientation relationship of $(111)_{GeSn}//(0001)_{Sapphire}$, $[110]_{GeSn}//[2\bar{1}\bar{1}0]_{Sapphire}$.

Fig. 4(d) shows another SAED pattern taken from multiple islands within the $Ge_{1-x}Sn_x$ uHTIL and sapphire substrate along the $[1\bar{1}00]$ axis of Al_2O_3. It presents a clean superposition pattern of the $[1\bar{1}00]$ zone Al_2O_3 (spots on the dashed rectangular lattice points) and the $[21\bar{1}]$ GeSn (spots off the dashed lattice). This observation confirms the formation of epitaxial GeSn islands on (0001) Al_2O_3. The GeSn islands and the substrate exhibit a clearly defined orientation relationship of $(111)_{GeSn}//(0001)_{Sapphire}$, $[1\bar{1}0]_{GeSn}//[2\bar{1}\bar{1}0]_{Sapphire}$, $[21\bar{1}]_{GeSn}//[1\bar{1}00]_{Sapphire}$.

Fig. 4(e) shows another XTEM image captured from a thick TEM foil of $Ge_{1-x}Sn_x$ uHTIL on (0001) sapphire, viewed at a 10° angle away from the $[2\bar{1}\bar{1}0]$ axis of Al_2O_3, clearly revealing the three-dimensional morphology of the epitaxial GeSn islands on the (0001) sapphire substrate.

The (111) GeSn planes exhibit a lattice spacing of 3.29 Å, corresponding a lattice constant 5.698 Å and Sn concentration of 5.1 at.%, with a -24% mismatch along the growth direction compared to the (0003) Al_2O_3 planes, which have a lattice spacing of 4.33 Å. Additionally, the (022) GeSn planes have a lattice spacing of 2.016 Å, corresponding a lattice constant 5.701Å and 5.5 at.% Sn, with a -15.3% mismatch along the interface direction with respect to the $(11\bar{2}0)$ Al_2O_3 planes, which possess a lattice spacing of 2.379 Å. EDS analysis, performed using a 10 nm nanobeam probe, reveals that the core area within a single island (refer to the core in Fig. 4(a)) exhibits a noticeably lower Sn content of 9-11 at.% (Fig. 4(f)) compared to the near-surface region of the islands (refer to the surface region in Fig. 4(a)), which has 30- 47 at.% Sn (Fig. 4(g)).

Fig. 5(a) shows a representative X-HRTEM image of the $Ge_{1-x}Sn_x$ uHTIL on (0001) sapphire substrate along the $[2\bar{1}\bar{1}0]$ of Al_2O_3. The image exhibits multiple types of GeSn twin domains (T_1, T_2 and T_3). The T_1 and T_2 (T_2^1, T_2^2 and T_2^3) domains share their (111) planes, which are aligned parallel to the interface plane. Meanwhile, the $(11\bar{1})$ of T_1 and $(1\bar{1}1)$ T_2 are misoriented by an angle of 23.8°, forming a boundary ($TB_{1,2}$) between them. The T_3 type twin domain, sandwiched between T_2^1 and T_2^2, is formed by sharing their $(1\bar{1}1)$ planes. The T_2^2 and T_2^3 domains are connected by a stacking fault (SF). All domains exhibit an atomically sharp, clear interface with the substrate.

Fig. 5(b) shows a X-HRTEM image of the GeSn/sapphire interface along the $[2\bar{1}\bar{1}0]$ axis of Al_2O_3, exhibiting well-aligned lattices between GeSn and sapphire with a clear, direct atomic correspondence at the interface. The left side of Fig. 5(c) shows an enlarged HRTEM image of the marked area in Fig. 5(b), overlaid with the projection of GeSn along the [110] direction and Al_2O_3 along the $[2\bar{1}\bar{1}0]$ direction, along with the corresponding simulated HRTEM images. This study, using high resolution electron microscopy combined with HREM image simulation, suggests that the bright dots in the HRTEM image of GeSn correspond to the GeSn motifs. The bright dots in the Al_2O_3 image correspond to the vacant channels within the structure, as indicated by the brown dots overlaid on the Al_2O_3 image. This study further indicates that the Al layer is the terminating layer or the outermost surface layer of the (0001) sapphire substrate. A possible atomic structure of the GeSn/sapphire is schematically illustrated on the right side of Fig. 5(c), where the large and small dots within Al_2O_3 represent Al and O atoms, respectively.

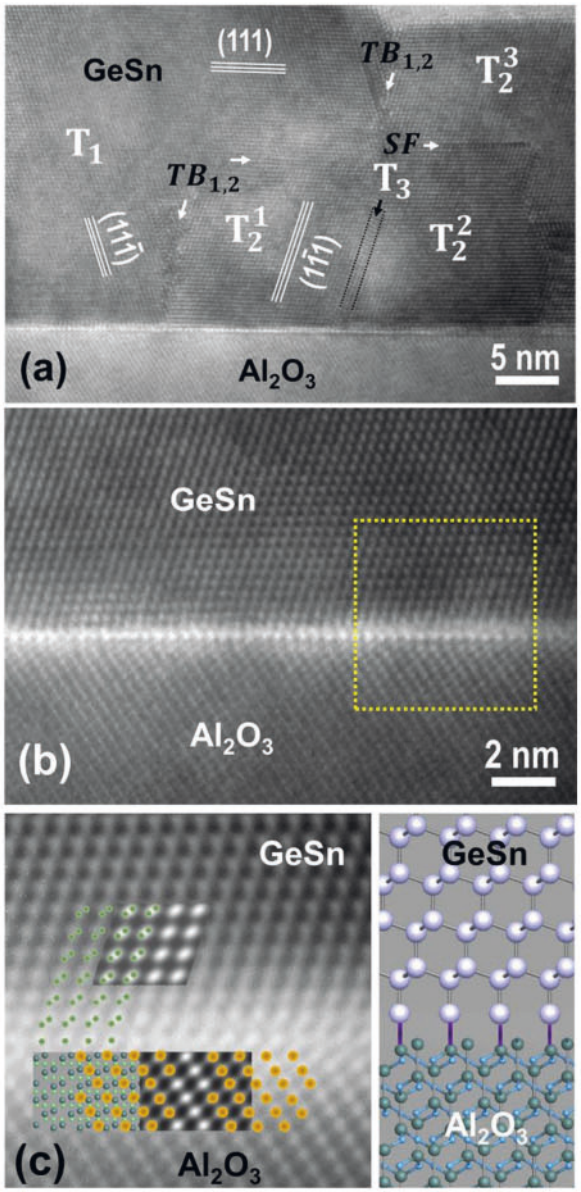

Fig. 5. (a) X-HRTEM image of $Ge_{1-x}Sn_x$ uHTIL on (0001) sapphire substrate along the $[2\bar{1}\bar{1}0]$ axis of Al_2O_3 direction, (b) X-HRTEM image of the GeSn/sapphire interface along the $[2\bar{1}\bar{1}0]$ axis of Al_2O_3, (c) enlarged HRTEM image of the marked area in (b) superposed with simulated HRTEM images of GeSn and Al_2O_3 and the projection of GeSn and Al_2O_3 along the $[2\bar{1}\bar{1}0]$ Al_2O_3 direction (left) and the schematic illustration of GeSn/sapphire interface structure (right) (large and small dots within Al_2O_3 represent Al and O atoms, respectively).

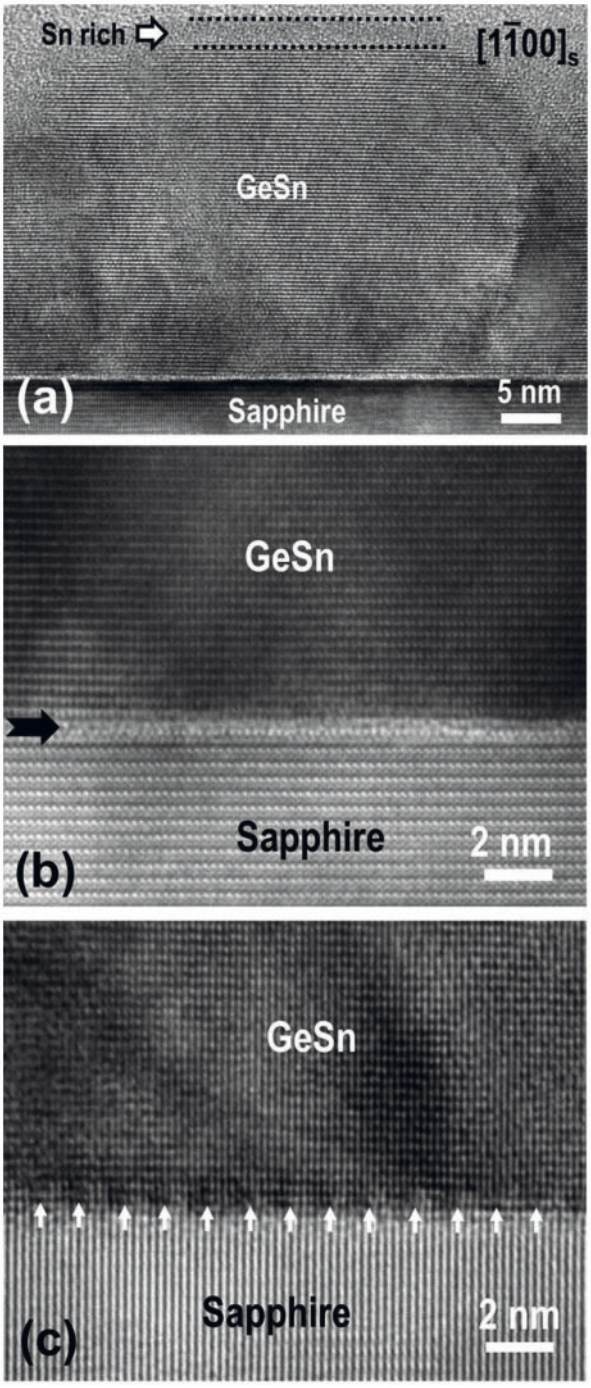

Fig. 6. (a) and (b) X-HRTEM image of the $Ge_{1-x}Sn_x$ uHTIL and the interface along the $[1\bar{1}00]$ axis of Al_2O_3, respectively. (c) X-HRTEM image of the GeSn/sapphire interface, taken using a diffraction condition with only $(h\ h\ \overline{2h}\ 0)$ Al_2O_3 and $(0\ 2k\ 2k)$ GeSn (h, k = ±1, ±2, ±3) diffractions being excited.

Fig. 6(a) exhibits a X-HRTEM image of a GeSn island in the uHTIL film, taken along the $[1\bar{1}00]$ axis of sapphire, clearly showing a GeSn epitaxial structure with a sharp interface. A dark amorphous layer, 2-4 nm thick (region between the two dashed lines), on top of the island corresponds to Sn-rich material. Fig. 6(b) shows a X-HRTEM image of the GeSn/sapphire interface taken along the $[1\bar{1}00]$ of the substrate, displaying lattices of GeSn well-aligned on sapphire. The GeSn/sapphire interface appears as a disrupted monolayer structure rather than a direct lattice connection between the film and the substrate. Fig. 6(c) shows a X-HRTEM image of the GeSn/sapphire interface, taken by tilting the $[1\bar{1}00]$ axis of Al_2O_3 away from the electron-beam. This tilting results in only $(h\ h\ \overline{2h}\ 0)Al_2O_3$ and $(0\ 2k\ 2k)$ GeSn (h, k = ±1, ±2, ±3) diffractions being excited. Fig. 6(c) exhibits quasi-periodically distributed edge dislocations (labeled by white arrows). The distance between adjacent misfit dislocations spans from five $(11\bar{2}0)$ Al_2O_3 or six (022) GeSn to six $(11\bar{2}0)$ Al_2O_3 or seven (022) GeSn crystallographic planes along

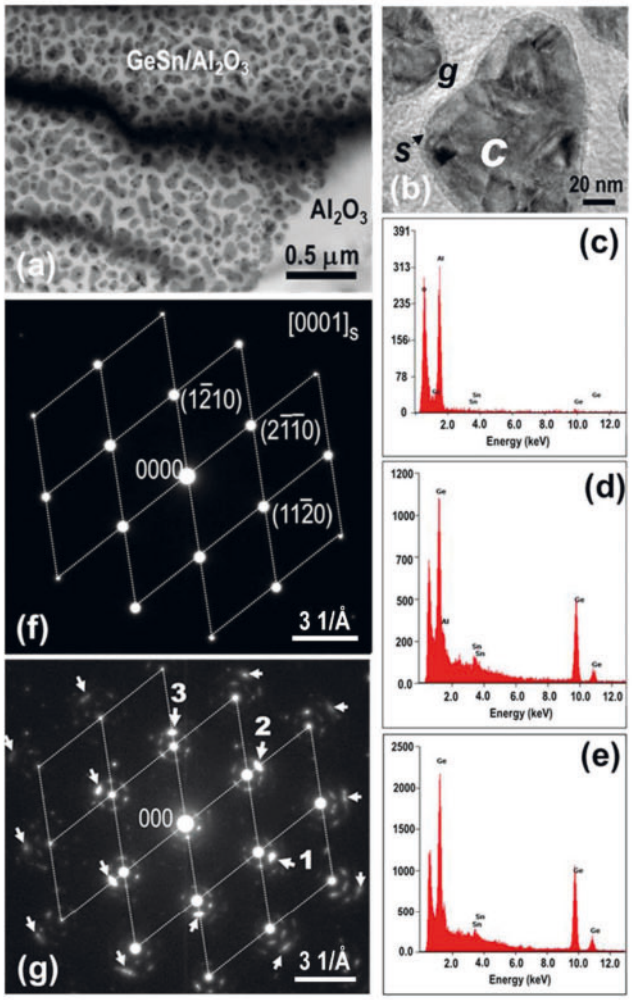

Fig. 7. (a) Plan-view TEM image of the $Ge_{1-x}Sn_x$ uHTIL/sapphire; (b) enlarged plan-view TEM image of the $Ge_{1-x}Sn_x$ uHTIL/sapphire; (c), (d), and (e) EDS spectra from the gap (*g*), the near-surface (*s*) and the core (*c*) region as depicted in (b), respectively. (f) and (g) SAED patterns from the substrate and the GeSn/sapphire interface, respectively; Subscript "s" in (f) indicates substrate.

the interface. This results in a high-density of misfit dislocations (~7 x10^7 dislocations/m) along the interface. This generates a monolayer-thick disrupted lattice image at the interface as shown in Fig. 6(b).

The GeSn island morphology and distribution on the film plane were studied by plan-view TEM of $Ge_{1-x}Sn_x$ uHTIL/sapphire by removing the substrate using ion-milling, Fig. 7(a). The dark domains enclosed by the white boundaries are indicative of GeSn structures, aligning with the islands shown in Fig. 4(a) and (e). Fig. 7(b) presents an enlarged TEM image for a detailed examination of the island structure. The GeSn islands have a width from 30 nm - 200 nm and possess indistinct shapes immersed in a bright matrix, while the white boundaries or gaps (regions labeled by "*g*" in Fig. 7(b)) between the islands correspond to Al_2O_3 substrate, measure between several nm to 60 nm. This observation has been verified through EDS analysis, as shown in Fig. 7(c), exhibiting only Al and O. The edges of the islands were encapsulated by a ~4 nm thick surface layer (regions labeled by "*s*" in Fig. 7(b)), exhibiting a higher Sn content ranging from 18-24 at.%, as obtained from EDS analysis (Fig. 7(d)). In contrast, the core region of the island (regions labeled by "*c*" in Fig. 7(b)) exhibits a lower Sn content, ranging from 8-15 at.% (Fig. 7(e)). The observation of the higher Sn content surface layer encapsulating the GeSn islands revealed by plan-view and XTEM - EDS studies is consistent with the elevated Sn content determined through XPS analysis. The lower Sn content revealed by Raman and diffraction analysis corresponds to the GeSn crystal structure.

Fig. 7(f) and (g) show SAED patterns taken from the substrate and the uHTIL GeSn/ sapphire interface in a plan-view TEM sample, respectively, along to the [0001] axis of Al_2O_3. Fig. 7(g) was taken from a region encompassing many GeSn islands in Fig. 7(a). In Fig. 7(g), the spots situated on the dashed lattice points correspond to the diffractions of the [0001] Al_2O_3, while those marked by arrows correspond to the diffractions of the [111] GeSn. The spots 1, 2 and 3 correspond to GeSn (220), (0$\bar{2}$2) and ($\bar{2}$02), respectively. The remaining spots correspond to the double diffractions produced by the overlap of the Al_2O_3 and GeSn at the interface. Fig. 7(g) distinctly displays a clean and well-defined superposition of the [0001] Al_2O_3 and [111] GeSn patterns serving as a further strong indicator of the epitaxial nature of GeSn islands on the sapphire substrate. The lattice mismatch between the (11$\bar{2}$0) Al_2O_3 the (220) GeSn measured in Fig. 7(g) is −15.1%, nearly identical to the value measured from the X-TEM (Fig. 4(d)).

Fig. 8(a) exhibits another magnified plan-view bright-field TEM image of the $Ge_{1-x}Sn_x$ uHTIL/sapphire with an SAED pattern inset. Fig. 8(b), (c) and (d) display dark-field images taken from the paired X ((220) GeSn-(11$\bar{2}$0) Al_2O_3), Y ((0$\bar{2}$2) GeSn-(2$\bar{1}\bar{1}$0) Al_2O_3), and Z (($\bar{2}$02) GeSn - (1$\bar{2}$10) Al_2O_3) diffractions in a near two-beam condition, respectively, exhibiting diffraction contrast images from the marked area in Fig. 8(a). Each individual dark-field image exhibits a series of parallel, periodically distributed fine black lines that are perpendicular to the corresponding diffraction vector. The average distance between the fine black lines is 13.3 Å. Each one of these lines represents an edge misfit dislocation at the GeSn/sapphire interface. This evidence shows that an edge misfit dislocation is formed every 13.3 Å at the GeSn/sapphire interface along the [11$\bar{2}$0] Al_2O_3 direction. The lattice spacing of the (220) GeSn planes is 2.015 Å, corresponding to a GeSn structure with a lattice constant 5.70 Å and 5.3 at.% Sn. A close examination showed that the spacing of the lines in the dark-field images is not uniform (up to 16% difference), as shown in the enlarged image in Fig. 8(e). The line spacing ranges from 14.3 Å (marked by L) to 11. 9 Å (marked by S). The large spacing signifies the coherent joining of seven GeSn (220) planes and six (11$\bar{2}$0) Al_2O_3 at the interface. In contrast, the small spacing indicates the coherent joining of six GeSn (220) planes and five (11$\bar{2}$0) Al_2O_3 at the interface, as schematically illustrated in Fig. 8(f). The lattice mismatch (δ) between the film and the substrate is −15.3%.

The interaction of three different oriented sets of edge dislocations generates a well-defined hexagonal modulated superlattice arrangement within the GeSn islands, as observed in the HRTEM image in Fig. 9(a). These arrangements bear a

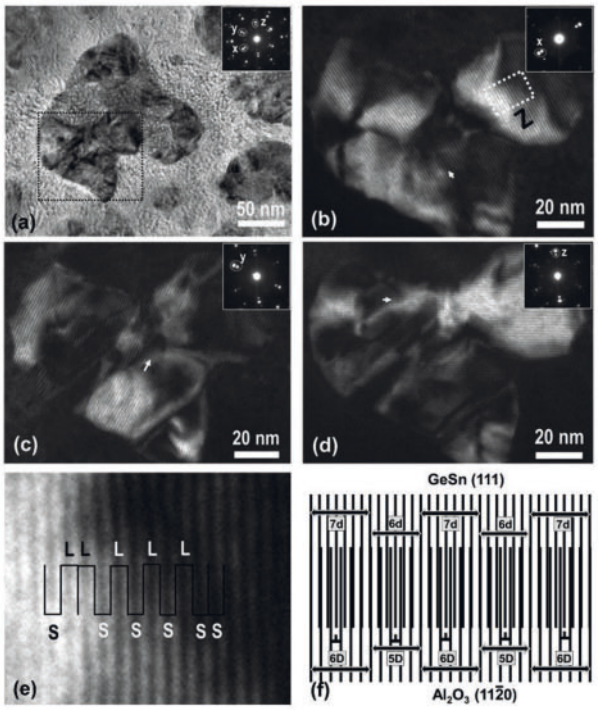

Fig. 8. (a) Plan-view bright-field TEM image of the $Ge_{1-x}Sn_x$ uHTIL/sapphire with an SAED pattern inset. (b), (c), and (d) dark-field images taken using diffraction spot X, Y and Z from the inset in (a), respectively. (e) Enlarged image of the area marked "Z" in (b). (f) Illustration of dislocations formation at the $Ge_{1-x}Sn_x$/ sapphire interface, with "⊥" in (f) indicating the locations of misfit dislocations. In (e), "L" and "S" represent the large and small spacings between the fringes, respectively. In (f), "d" and "D" represent the lattice spacings of the GeSn (111) and Al_2O_3 (11$\bar{2}$0) planes, respectively.

resemblance to patterns observed in HRTEM images in our previous studies of epitaxial films [34], [35], [36], [37], [38]. The formation of the hexagonal modulated structure and misfit dislocation network at the interface is schematically illustrated in Fig. 9(b), by overlapping the projections of GeSn along the [111] direction and of Al_2O_3 along the [0001] direction, aligned with $[21\bar{1}]_{GeSn}$//$[1\bar{1}00]_{Sapphire}$, $[1\bar{1}0]_{GeSn}$ // $[11\bar{2}0]_{Sapphire}$. The lighter gap region in Fig. 9(a) lacking this modulated structure corresponds to the sapphire substrate.

C. TEM Studies of $Ge_{1-x}Sn_x$ LTTF on (0001) Sapphire Substrate

The X-TEM study reveals that the $Ge_{1-x}Sn_x$ LTTF on (0001) sapphire substrate exhibits a columnar-like structure (~900 nm thick) atop a solid layer (~tens of nm), as shown Fig. 10(a). Fig. 10(b) shows an enlarged cross-section TEM image of the GeSn/sapphire interface, where the GeSn regions near the substrate exhibit the formation of numerous twin structures, similar to the structure observed in our previous studies on epitaxial films [34], [35], [39], [40]. The top columnar section of the $Ge_{1-x}Sn_x$ LTTF consists of nanocrystalline GeSn, as identified by SAED analysis, shown in Fig. 10(c). The rings α, β, and γ in Fig. 10(c) correspond to the diffractions (111), (220) and (311) of GeSn. Not all (111) diffraction spots lie exactly on

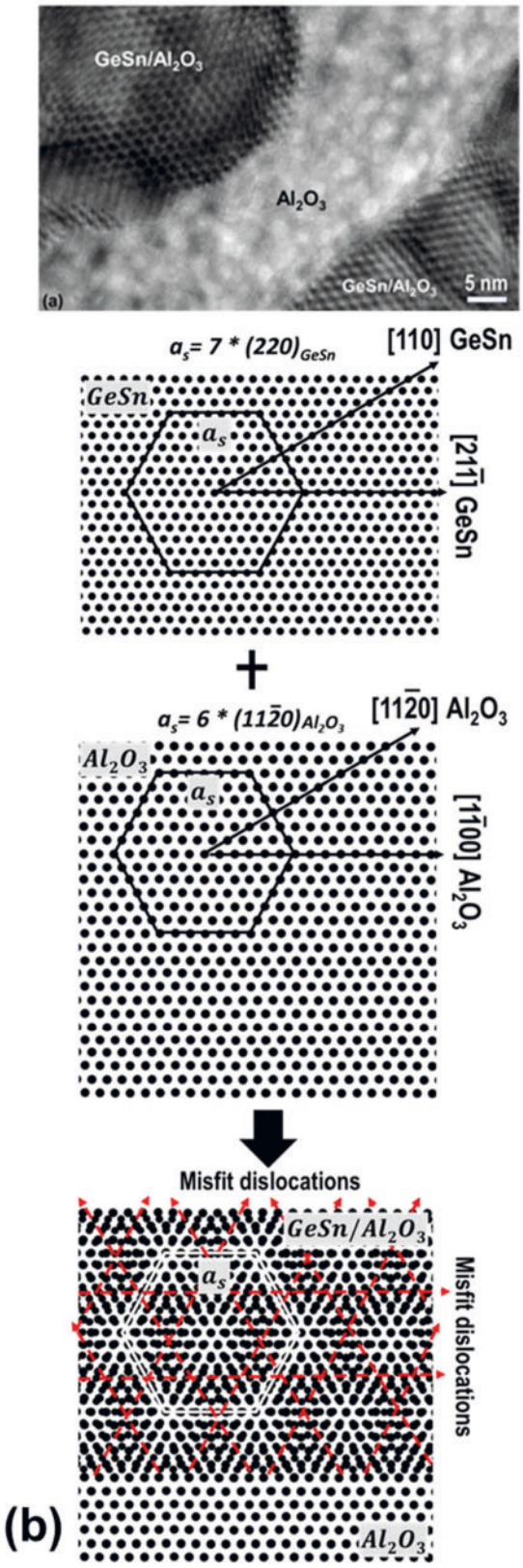

Fig. 9. (a) Plan-view HRTEM image from a region covering island and open space of the GeSn uHTIL/sapphire, (b) illustration of the formation of 2-D superlattice at the GeSn/sapphire interface.

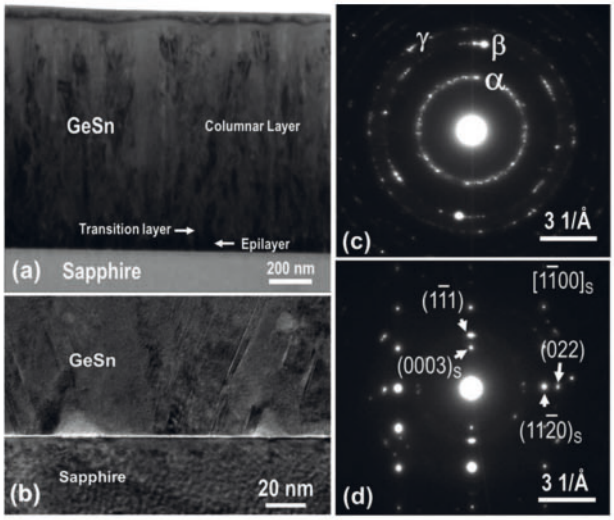

Fig. 10. (a) XTEM image of the entire $Ge_{1-x}Sn_x$ LTTF on (0001) sapphire substrate, (b) magnified XTEM image near the GeSn/sapphire interface; (c) SAED pattern from the top region of the film, (d) SAED pattern of the GeSn/sapphire interface along the $[1\bar{1}00]$ Al_2O_3 direction.

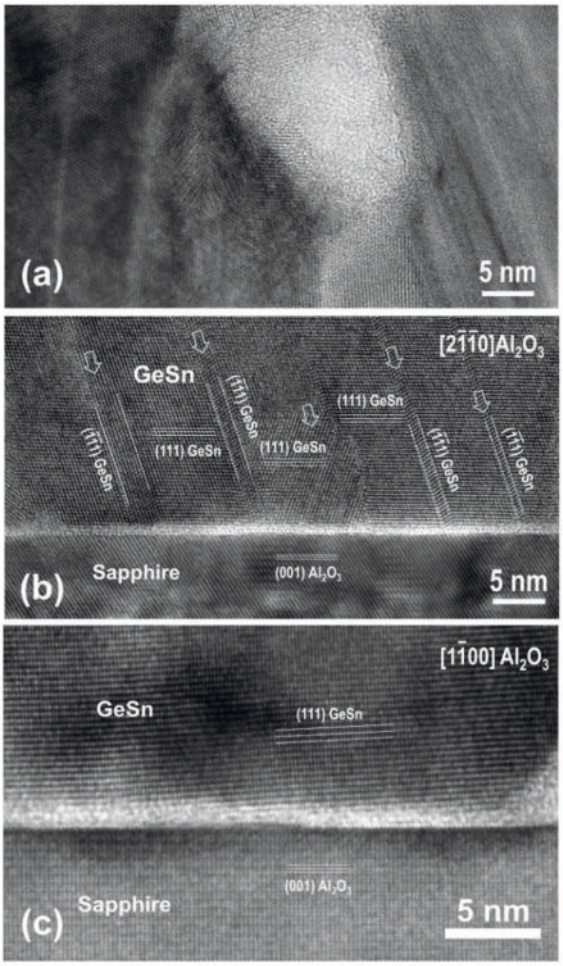

Fig. 11. (a) X-HRTEM image of the top region of the $Ge_{1-x}Sn_x$ LTTF on sapphire substrate, (b) and (c) X-HRTEM images of the GeSn/sapphire interface along the $[2\bar{1}\bar{1}0]$ and $[1\bar{1}00]$ Al_2O_3 direction, respectively.

circles with the same radius, indicating a variety of lattice spacing, varying from of 3.31 Å to 3.33 Å, corresponding to crystalline GeSn with lattice constants measured from 5.74 Å to 5.77 Å, representing Sn incorporation of 11 at.% to 14 at.%, respectively. This indicates that GeSn crystallites with different Sn concentrations were formed in the top columnar layer of the film, similar to the structure observed in GeSn films grown on Si substrate [35]. The solid, dark GeSn layer near the interface, in Fig. 10(a), has an epitaxial structure implanted with some twin structures, as revealed by SAED. Fig. 10(d) shows a SAED pattern taken from the GeSn/sapphire interface along the $[1\bar{1}00]$ axis of Al_2O_3. The GeSn (111) planes, Fig. 10(d), exhibit a lattice spacing of 3.29 Å, corresponding to a GeSn structure with a Sn concentration of 5.3 at.% and a lattice constant 5.70 Å, with a mismatch of -24% along the growth direction compared to the (0003) Al_2O_3 planes. The (022) GeSn planes perpendicular to the interface have a lattice spacing of 2.012 Å, corresponding a lattice constant: a = 5.69 Å, and 4.1 at.% Sn, representing a -15.5% mismatch with respect to the $(11\bar{2}0)$ Al_2O_3 planes. The mismatch level is identical to the one obtained for the uHTIL GeSn on sapphire substrate. SAED studies show that the concentration in the epitaxial layer is slightly lower than that in the columnar layer. This observation is also confirmed by the EDS analysis. The orientation relationship between the GeSn epitaxial structure and the (0001) sapphire substrate in $Ge_{1-x}Sn_x$ LTTF is identical to that in $Ge_{1-x}Sn_x$ uHTIL.

Fig. 11(a) displays a X-HRTEM image of the top region of the $Ge_{1-x}Sn_x$ LTTF exhibiting a columnar structure with poly-crystalline GeSn. Fig. 11(b) and (c) show X-HRTEM images of the GeSn/sapphire interface along the $[2\bar{1}\bar{1}0]$ and $[1\bar{1}00]$ Al_2O_3 direction, respectively. Both images clearly illustrate the (111) GeSn planes within the epitaxial structure aligned nearly parallel to the (0001) Al_2O_3, along with an amorphous layer measuring $\sim$ 1 nm at the interface between the GeSn film and sapphire substrate. GeSn nanotwins (marked by arrows) sharing their $(\bar{1}\bar{1}1)$ planes with the epitaxial counterpart are also present in Fig. 11(b).

The microstructure evolution of the $Ge_{1-x}Sn_x$ LTTF in a layer-by-layer manner along the growth direction is further studied by plan-view TEM. Fig. 12(a) and (b) show a plan-view, bright-field TEM image and the corresponding SAED pattern of the top columnar layer of the film, respectively. This layer was isolated by eliminating the substrate and bottom layer using ion-milling. The cross-sections of the columnar structure exhibit nearly equal axis grains with sizes ranging from 70 – 130 nm. The crystallographic orientations of those grains are randomly arranged, as revealed by the SAED pattern shown in Fig. 12(b). GeSn nano-twins were frequently observed within the columnar structures, as shown in Fig. 12(c), which is an HRTEM image of the black grain marked with an asterisk (∗) in Fig. 12(a).

Fig. 13(a) and (b) show a plan-view, bright-field TEM image and the corresponding SAED pattern of a transition layer in the $Ge_{1-x}Sn_x$ LTTF film on (0001) sapphire substrate, respectively. This transition layer, which shifts from the bottom epitaxial to the upper nanocrystalline structure, corresponds to the layer depicted in Fig. 10(a). This layer predominantly consists of a single crystal epitaxial configuration in conjunction with twins, as demonstrated by the SAED pattern shown in Fig. 13(b). These

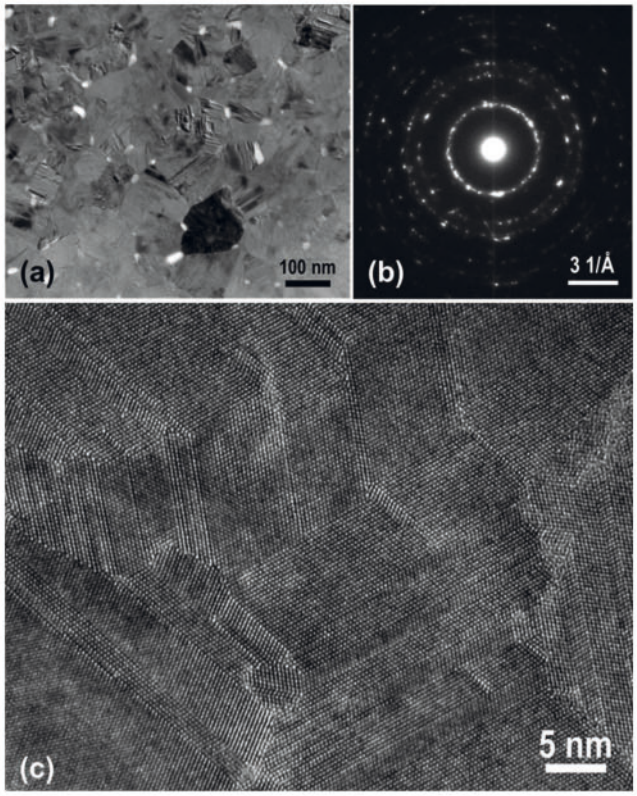

Fig. 12. (a) Plan-view TEM image, (b) SAED pattern, and (c) plan-view HRTEM image from the top layer of $Ge_{1-x}Sn_x$ LTTF on (0001) sapphire substrate.

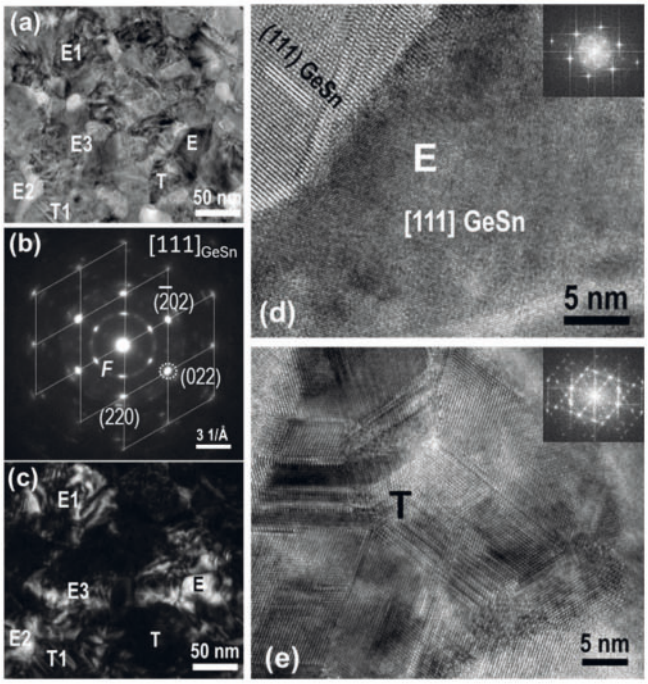

Fig. 13. (a) Bright-field TEM image, (b) SAED pattern, (c) dark-field image, (d) and (e) HRTEM images from epitaxial (E) and twin (T) regions in (a) or (c), in a plan-view transition layer from the bottom epitaxial to up nanocrystalline structure in the $Ge_{1-x}Sn_x$ LTTF on sapphire substrate.

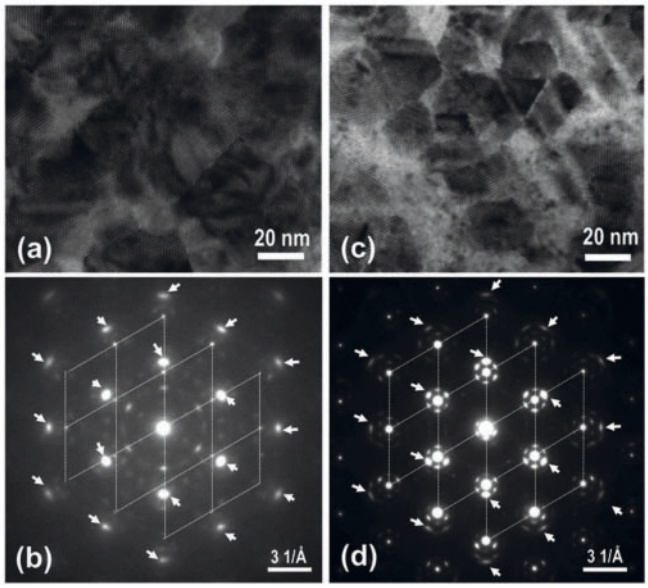

Fig. 14. TEM image and SAED pattern of (a) and (b) the bottom layer near the interface and (c) and (d) the interface from a plan-view sample of $Ge_{1-x}Sn_x$ LTTF on sapphire substrate.

strong diffraction spots positioned at the dashed lattice points correspond to diffractions observed in the [111] GeSn zone diffraction pattern of the epitaxial crystal. The remaining spots align with the diffractions observed in the diffraction patterns of the GeSn twins. For example, spots positioned at the first ring (labeled as "*F*" in Fig. 13(b)) correspond to the (111) of GeSn twins. Fig. 13(c) displays a dark-field image taken from the (022) GeSn diffraction under a near two-beam condition. The predominant white contrast regions (such as E, E1, E2 and E3) demonstrate the presence of the epitaxial structure, whereas the black contrast regions, such as T and T1, signify twin structures.

Such composite structure of the transition layer has been further investigated and confirmed using HRTEM. Fig. 13(d) and (e) show HRTEM images from the epitaxial (E) and twin (T) regions in Fig. 13(a), respectively. These images clearly reveal an epitaxial [111] GeSn single crystal in the former and [111] GeSn twins in the latter. Fig. 13(d) also displays the direct connection of the GeSn (111) twin to the GeSn epitaxial grain.

Fig. 14(a) shows a bright-field TEM image of the GeSn epitaxial layer in a plan-view sample of $Ge_{1-x}Sn_x$ LTTF on (0001) sapphire substrate. The sample was prepared by selectively removing the GeSn columnar crystalline material from the film side and a substantial portion of the sapphire from the substrate side, leaving behind a very thin sapphire layer through ion-milling. In this image, the GeSn layer is significantly thicker than the sapphire layer, and the electron beam is aligned parallel to the [0001] axis of Al_2O_3, or the [111] axis of the GeSn. This TEM image unequivocally demonstrates the well-defined hexagonal lattice in conjunction with parallel lattice fringes, the former corresponds to presence of [111] epitaxial crystal and the latter indicates GeSn twins. Fig. 14(b) displays an SAED pattern corresponding to the region shown in in Fig. 14(a). The weak sharp spots in this pattern, located at the dashed

lattice points, correspond to the diffraction spots observed in the [0001] zone of Al_2O_3. The strong spots marked by arrows correspond to the diffractions observed in the [111] zone of GeSn epitaxial structure. The remaining weak spots correspond to the diffractions from twins and double diffractions resulting from the overlapping interference of GeSn and Al_2O_3. The lattice spacing of (220) GeSn in the epilayer is 2.016 Å, corresponding to a GeSn with a lattice constant of 5.70 Å, indicating formation of $Ge_{0.95}Sn_{0.05}$ The lattice spacing of (111) planes of GeSn twins is 3.32 Å, corresponding to a lattice constant of 5.74 Å, indicating formation of $Ge_{0.9}Sn_{0.1}$. This shows that the GeSn twins contain higher Sn content compared to the GeSn epilayer.

Fig. 14(c) and (d) show a TEM image and an SAED pattern, respectively, taken from a plan-view interface where the GeSn layer and the sapphire layer have nearly the same thickness. These images were captured under identical imaging conditions to Fig. 14(a) and (b). In Fig. 14(d), the spots corresponding to the diffraction observed in the [0001] zone of Al_2O_3, located at the dashed lattice points, and the double diffraction exhibit a significantly enhanced intensity, nearly matching that of the diffraction observed in the [111] zone of GeSn, as labeled by the arrows. The lattice spacing of the GeSn (220) in Fig. 14(d) is 2.010 Å, corresponding to a lattice constant of 5.68 Å, indicating formation of $Ge_{0.97}Sn_{0.03}$. The results in Fig. 14(a)–(d) indicate that the epitaxial GeSn closer to the sapphire substrate contains less Sn than the structure far from the substrate. The lattice mismatch between (220) GeSn and $(11\bar{2}0)$ Al_2O_3 at the interface is −15.4%. The TEM image, as shown in Fig. 14(c), displays well-defined multifaceted domains (such as triangular, quadrilateral or polygon shapes) with hexagonal lattice, corresponding to epitaxial GeSn. Occasionally, certain regions exhibit a series of parallel lattice fringes, indicating the existence of GeSn twins. These hexagonal lattice domains have an average size of ∼20 nm, notably smaller than those shown in Fig. 14(a). This indicates that the GeSn epitaxial domains undergo rapid lateral growth and coarsening during the initial stages of film formation.

Fig. 15(a) shows a HRTEM image captured from a plan-view sample at the LTTF $Ge_{1-x}Sn_x$/sapphire interface, exhibiting three distinct characteristics. In this image, the clean region (indicated by Al_2O_3) with fine lattices corresponds to the pure sapphire substrate. Its fast Fourier transformation (FFT) is displayed in Fig. 15(b), revealing a pattern identical to the one observed for the [0001] zone of Al_2O_3. The regions with well-defined hexagonal modulated superlattice arrangements, such as the one indicated by ET, correspond to the (111) GeSn epitaxial structure. Its FFT is shown in Fig. 15(c), revealing a pattern identical to the observed SAED pattern of the plan-view GeSn/sapphire interface, as shown in Figs. 7(g) and 14(d). The modulation wavelength, measures approximately 13.1 Å along three equivalent close-packed directions, i.e., $[11\bar{2}0]$, $[2\bar{1}10]$ and $[1\bar{2}10]$ of Al_2O_3. This spacing signifies the coherent joining of the (220) GeSn and $(11\bar{2}0)$ Al_2O_3 planes at the interface every 13.1 Å. As a result, approximately 13 (220) planes of GeSn align with 11 $(11\bar{2}0)$ planes of Al_2O_3, revealing a calculated lattice mismatch of −15.4% at the interface. Estimation indicates a Sn content of approximately 3 at.% within the GeSn layer at the interface. The regions displaying a series of parallel fringes,

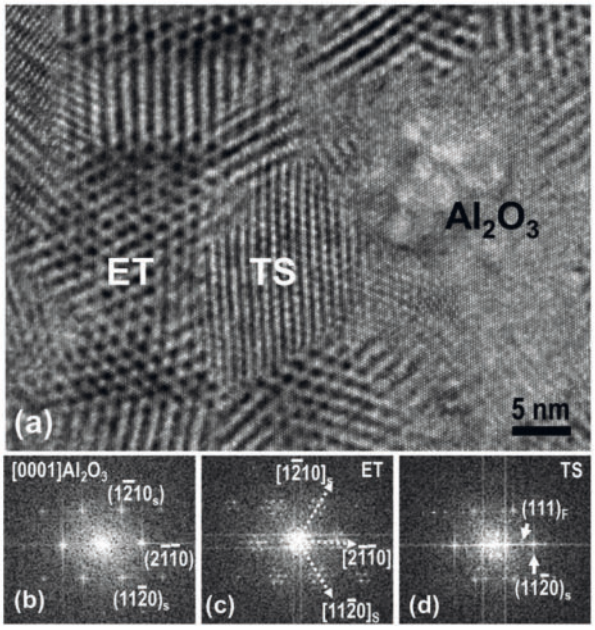

Fig. 15. (a) HRTEM of the interface from a plan-view sample of $Ge_{1-x}Sn_x$ LTTF on sapphire substrate. (b)–(d) FFT from the Al_2O_3, TS and ET regions in (a). Subscripts "S" and "F" indicate substrate and film, respectively.

such as the one indicated by TS, correspond to the GeSn twins with their (111) plane vertically aligned and grown on (0001) Al_2O_3 substrate. Its FFT is shown in Fig. 15(d), revealing (111) GeSn with a lattice spacing of 3.33 Å, corresponding to GeSn with a Sn content of ∼14 at.% and a lattice constant of 5.77 Å. The twins exhibit a higher Sn content than the epitaxial structure, consistent with the results extracted from the SAED pattern. In twins, approximately 5 (111) planes of GeSn align with 7 $(11\bar{2}0)$ planes of Al_2O_3 and two misfit dislocations are formed every 16.6 Å to accommodate the lattice mismatch strain between these two structures.

D. Discussion

The microstructures of the $Ge_{1-x}Sn_x$ uHTIL and LTTF films as revealed by the TEM studies are schematically summarized in Fig. 16. The $Ge_{1-x}Sn_x$ uHTIL deposited on (0001) sapphire substrate at 475 °C exhibits a discrete island morphology. The formation of such an island morphology follows a similar mechanism scenario to the case of GeSn islands directly deposited on (001) Si [34]. However, in this work, the morphology of each GeSn island appears as a mushroom-like morphology with the bottom of the island connected to the substrate, exhibiting a narrowed neck. In this film, the (220) GeSn planes at the interface exhibit a lattice mismatch of −15.3% with the $(11\bar{2}0)$ of Al_2O_3, corresponding to a Sn content of approximately ∼5.3%. The GeSn lattice experiences strong tensile strain on the film plane, forcing the GeSn lattice to expand along the interface direction. The strain relaxation caused by this lattice expansion attracts large Sn atoms and results in incorporation of more Sn in the core region. However, the lattice is not well connected to the substrate. Additional Sn causes the amorphization at the interface. On the other hand, the lattice spacing of the GeSn crystal planes

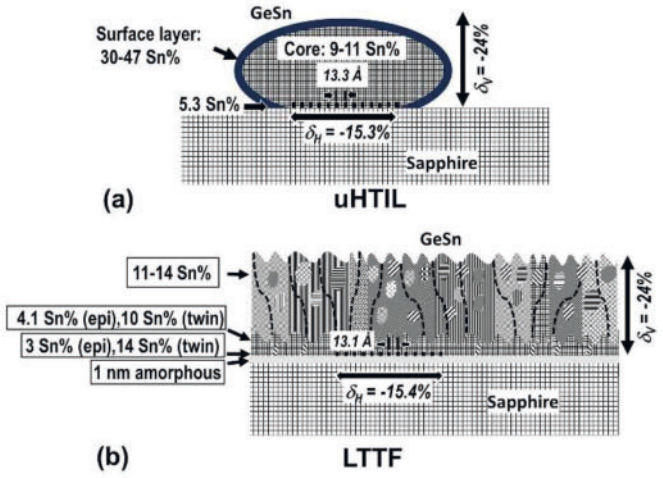

Fig. 16. Schematic illustration of the microstructures of the $Ge_{1-x}Sn_x$ uHTIL (a) and LTTF (b). epi: Epilayer; H: Horizontal; V: Vertical.

is notably smaller than those of the coherently aligned lattice planes to the sapphire substrate. On (0001) sapphire, epitaxial GeSn films with higher Sn content exhibit smaller lattice mismatch and, consequently, smaller misfit strain with the substrate. Therefore, it may be less challenging to deposit epitaxial GeSn films with high Sn content on (0001) sapphire substrates. The $Ge_{1-x}Sn_x$ uHTIL deposited on the (0001) sapphire substrate exhibits a clear, atomically sharp interface, where the GeSn lattice coherently joins the Al atoms on the substrate surface. This indicates that the lattice misfit strain at the GeSn/sapphire interface was effectively accommodated, thereby significantly reducing residual strain within the GeSn epilayer. This structure can act as a precursor for subsequent epitaxial deposition of thick GeSn film.

The $Ge_{1-x}Sn_x$ LTTF on (0001) sapphire deposited at 367 °C is composed of an epilayer (or (111) orientation preferred structure) on the substrate which transitions to an upper columnar nanocrystalline layer. This film has an amorphous or disrupted structure layer measuring approximately 1 nm at the interface, in contrast to the clear, atomically sharp, coherently joined interface in the $Ge_{1-x}Sn_x$ uHTIL. This observation indicates that increasing the deposition temperature can improve the interface between the GeSn film and the sapphire substrate. In the $Ge_{1-x}Sn_x$ LTTF, the epilayer near the substrate exhibits a higher density of twins compared to the $Ge_{1-x}Sn_x$ uHTIL. This is due to the lower growth temperature for the $Ge_{1-x}Sn_x$ LTTF compared to the $Ge_{1-x}Sn_x$ uHTIL. The quality of the epilayer degrades along the growth direction. The Sn content in the GeSn epilayer near the substrate is lower than that in regions farther from the interface and increases as the film continues to grow. Such a composition and structural gradient is suspected to result from the lower deposition temperature. Increasing the deposition temperature is anticipated to improve the quality of the GeSn epitaxial layer. It is also observed that the epitaxial $Ge_{1-x}Sn_x$ uHTIL deposited on (0001) sapphire substrate at 475 °C contains nearly identical or even slightly higher Sn content than the epilayer in the $Ge_{1-x}Sn_x$/sapphire deposited 367 °C. Increasing deposition temperature (from 367 °C to 475 °C) is expected to improve the epitaxial quality of the films while maintaining the same Sn content, and provides significant benefits for producing thicker, high-quality epitaxial GeSn thin films on sapphire substrates.

V. Conclusion

Detailed examinations and analysis are presented of epitaxial structures in an ultra-thin $Ge_{1-x}Sn_x$ uHTIL and a ~1 μm thick $Ge_{1-x}Sn_x$ LTTF films grown directly on (0001) sapphire substrates by RPECVD. The $Ge_{1-x}Sn_x$ uHTIL contains discrete mushroom-like epitaxial islands with a height ranging from 30-45 nm and a lateral width ranging from 40 - 200 nm. The GeSn islands are covered by a ~4 nm thick layer of Sn-rich amorphous material. The $Ge_{1-x}Sn_x$ LTTF contains an initial epilayer, tens of nm thick, below a ~900 nm upper columnar nanocrystalline structure. The epitaxial structures in both films have an orientation relationship of $(111)_{GeSn}//(0001)_{Sapphire}$, $[1\bar{1}0]_{GeSn}//[2\bar{1}\bar{1}0]_{Sapphire}$, $[21\bar{1}]_{GeSn}//[1\bar{1}00]_{Sapphire}$ with the substrate. The epitaxial structures in both films feature nano twins and exhibit lattice mismatches of ~15% between the (220) GeSn and the $(11\bar{2}0)$ Al_2O_3 along the interface plane and −24% between the (111) GeSn and the (0003) Al_2O_3 planes along the film growth direction. The high density of misfit dislocations at the interface plane is compensated by the formation of a quasiperiodic hexagonal network of misfit dislocations, with periodic lengths of 13.3 Å for $Ge_{1-x}Sn_x$ uHTIL/sapphire and 13.1 Å for $Ge_{1-x}Sn_x$ LTTF/sapphire. The GeSn/sapphire interfaces are characterized by a clear, atomically sharp structure in the $Ge_{1-x}Sn_x$ uHTIL sample, and a highly disrupted, nearly amorphous, ~1 nm thick layer in $Ge_{1-x}Sn_x$ LTTF. The nanocrystalline grains in the upper columnar regions of $Ge_{1-x}Sn_x$ LTTF have varying Sn content, with all concentrations higher than that observed in the epitaxial region. No Sn precipitates were observed in the film. Growing GeSn on (0001) sapphire substrates at a higher temperature results in an atomically sharp and robust interface and enhances epitaxial quality, while maintaining the Sn content level. This method is expected to provide significant advantages for producing thicker, high-quality epitaxial GeSn thin films directly on (0001) sapphire substrates.

References

[1] E. R. Dobrovinskaya, L. A. Lytvynov, and V. Pishchik, "Properties of sapphire," in *Sapphire: Material, Manufacturing, Applications (Micro- and Opto-Electronic Materials, Structures, and Systems)*, 1st ed. New York, NY, USA, Springer, 2009, pp. 55–176.

[2] T. Nakasu et al., "Surface texture and crystallinity variation of ZnTe epilayers grown on the step-terrace structure of the sapphire substrate," *J. Electron. Mater.*, vol. 45, pp. 2127–2132, 2016.

[3] P. Pirouz, F. Ernst, and Y. Ikuhara, "On epitaxy and orientation relationships in bicrystals," *Solid State Phenomena*, vol. 59, pp. 51–62, 1998.

[4] E. Wangila et al., "Single crystalline Ge thin film growth on c-plane sapphire substrates by molecular beam epitaxy (MBE)," *CrystEngComm*, vol. 24, no. 24, pp. 4372–4380, 2022.

[5] A. J. Duzik and S. H. Choi, "Low temperature rhombohedral single crystal SiGe epitaxy on c-plane sapphire," in *Proc. Nanosensors, Biosensors, Info-Tech. Sensors Syst.*, 2016, vol. 9802, pp. 48–58.

[6] H.-J. Kim, H.-B. Bae, Y. Park, K. Lee, and S. H. Choi, "Temperature dependence of crystalline SiGe growth on sapphire (0001) substrates by sputtering," *J. Cryst. Growth*, vol. 353, no. 1, pp. 124–128, 2012.

[7] W. B. Dubbelday and K. L. Kavanagh, "The growth of SiGe on sapphire using rapid thermal chemical vapor deposition," *J. Cryst. Growth*, vol. 222, no. 1/2, pp. 20–28, 2001.

[8] Y. Park, G. C. King, and S. H. Choi, "Rhombohedral epitaxy of cubic SiGe on trigonal c-plane sapphire," *J. Cryst. Growth*, vol. 310, no. 11, pp. 2724–2731, 2008.

[9] Z. Yang et al., "In situ relaxed $Si_{1-x}Ge_x$ epitaxial layers with low threading dislocation densities grown on compliant Si-on-insulator substrates," *J. Vac. Sci. Technol. B: Microelectronics Nanometer Struct. Process., Meas., Phenomena*, vol. 16, no. 3, pp. 1489–1491, 1998.
[10] S. J. Mathew, G. Niu, W. B. Dubbelday, and J. D. Cressler, "Characterization and profile optimization of SiGe pFETs on silicon-on-sapphire," *IEEE Trans. Electron Devices*, vol. 46, no. 12, pp. 2323–2332, Dec. 1999.
[11] J. Zuniga-Perez, R. Tena-Zaera, and V. Munoz-Sanjose, "Structural characterization of CdTe layers grown on (0 0 0 1) sapphire by MOCVD," *J. Cryst. Growth*, vol. 270, no. 3/4, pp. 309–315, 2004.
[12] T. P. Humphreys et al., "Heteroepitaxial growth and characterization of GaAs on silicon-on-sapphire and sapphire substrates," *Appl. Phys. Lett.*, vol. 54, no. 17, pp. 1687–1689, 1989.
[13] S. K. Saha et al., "Crystalline GaAs thin film growth on a c-plane sapphire substrate," *Cryst. Growth Des.*, vol. 19, no. 9, pp. 5088–5096, 2019.
[14] S. Wirths et al., "Lasing in direct-bandgap GeSn alloy grown on Si," *Nat. Photon.*, vol. 9, pp. 88–92, 2015, doi: 10.1038/NPHOTON.2014.321.
[15] S. Gupta, B. Magyari-Köpe, Y. Nishi, and K. Saraswat, "Achieving direct band gap in germanium through integration of Sn alloying and external strain," *J. Appl. Phys.*, vol. 113, 2013, Art. no. 073707.
[16] J. Mathews et al., "Direct-gap photoluminescence with tunable emission wavelength in Ge1-ySny alloys on silicon," *Appl. Phys. Lett.*, vol. 97, 2010, Art. no. 221912.
[17] Y. Zhou et al., "Electrically injected GeSn lasers on Si operating up to 100 K," *Optica*, vol. 7, pp. 924–928, 2020.
[18] Y. Zhou et al., "Optically pumped GeSn lasers operating at 270 K with broad waveguide structures on Si," *ACS Photon.*, vol. 6, pp. 1434–1441, 2019.
[19] J. Chrétien et al., "GeSn lasers covering a wide wavelength range thanks to uniaxial tensile strain," *ACS Photon.*, vol. 6, pp. 2462–2469, 2019.
[20] S. Zaima et al., "Growth and applications of GeSn-related group-IV semiconductor materials," *Sci. Technol. Adv. Mater.*, vol. 16, 2015, Art. no. 043502.
[21] R. Olesinski and G. Abbaschian, "The Ge-Sn (germanium-tin) system," *Bull. Alloy Phase Diagrams*, vol. 5, pp. 265–271, 1984.
[22] G. Grzybowski, M. E. Ware, A. Kiefer, and B. Claflin, "Design of a remote plasma-enhanced chemical vapor deposition system for growth of tin containing group-IV alloys," *J. Vac. Sci. Technol. B*, vol. 38, 2020, Art. no. 062209.
[23] B. Claflin, G. J. Grzybowski, M. E. Ware, S. Zollner, and A. M. Kiefer, "Process for growth of group-IV alloys containing tin by remote plasma enhanced chemical vapor deposition," *Front. Mater.*, vol. 7, 2020, Art. no. 44.
[24] J. Segura-Ruiz et al., "Impact of the growth strategy and device fabrication on the alloy homogeneity in optoelectronic grade Sn-rich GeSn," *Mater. Sci. Eng. B*, vol. 264, 2021, Art. no. 114899.
[25] H. Stanchu et al., "X-ray diffraction study of strain relaxation, spontaneous compositional gradient, and dislocation density in GeSn/Ge/Si (100) heterostructures," *Semicond. Sci. Technol.*, vol. 35, 2020, Art. no. 075009.
[26] S. Assali, J. Nicolas, and O. Moutanabbir, "Enhanced Sn incorporation in GeSn epitaxial semiconductors via strain relaxation," *J. Appl. Phys.*, vol. 125, 2019, Art. no. 025304.
[27] Y. Miao et al., "Characterization of crystalline GeSn layer on tensile-strained Ge buffer deposited by magnetron sputtering," *Mater. Sci. Semicond.*, vol. 85, pp. 134–140, 2018.
[28] W. Dou et al., "Investigation of GeSn strain relaxation and spontaneous composition gradient for low-defect and high-Sn alloy growth," *Sci. Rep.*, vol. 8, 2018, Art. no. 5640.
[29] D. Gayakwad et al., "Epitaxial growth of $Ge_{1-x}Sn_x$ on c–plane sapphire substrate by molecular beam epitaxy," *J. Cryst. Growth*, vol. 618, 2023, Art. no. 127306.
[30] G. Pilania et al., "Revisiting the Al/Al_2O_3 interface: Coherent interfaces and misfit accommodation," *Sci. Rep.*, vol. 4, no. 1, 2014, Art. no. 4485.
[31] P. A. Stadelmann, "EMS-a software package for electron diffraction analysis and HREM image simulation in materials science," *Ultramicroscopy*, vol. 21, no. 2, pp. 131–145, 1987.
[32] V. R. D'Costaa et al., "Raman scattering in $Ge_{1-y}Sn_y$ alloys," *Solid State Commun.*, vol. 14, pp. 240–244, 2007.
[33] J. Thapa, B. Liu, S. D. Woodruff, B. T. Chorpening, and M. P. Buric, "Raman scattering in single-crystal sapphire at elevated temperatures," *Appl. Opt.*, vol. 56, no. 31, pp. 8598–8606, 2017.
[34] J. Jiang et al., "Temperature-dependent morphology and composition of ultra-thin GeSn epilayers prepared by remote plasma enhanced chemical vapor deposition," *J. Vac. Sci. Technol. B*, vol. 42, no. 3, 2024.
[35] J. Jiang et al., "Epitaxial twin coupled microstructure in GeSn films prepared by remote plasma enhanced chemical vapor deposition," *J. Appl. Phys.*, vol. 135, no. 16, 2024.
[36] J. C. Jiang et al., "Two-dimensional interface structures of epitaxial $(Ba,Sr)TiO_3$ film on miscut (001) MgO," *Thin Solid Films*, vol. 518, pp. 147–153, 2009.
[37] J. C. Jiang et al., "Two-dimensional modulated interfacial structures of highly epitaxial ferromagnetic $(La,Ca)MnO_3$ and ferroelectric $(Pb,Sr)TiO_3$ thin films on (001) MgO," *J. Nano Res.*, vol. 3, pp. 59–66, 2008.
[38] J. C. Jiang, E. I. Meletis, Z. Yuan, and C. L. Chen, "Interface modulated structure of highly epitaxial $(Pb,Sr)TiO_3$ thin films on (001) MgO," *Appl. Phys. Lett.*, vol. 90, 2007, Art. no. 051904.
[39] J. He et al., "Twin-coupled domain structures in epitaxial relaxor ferroelectric Ba (Zr,Ti) O_3 thin films on (001) MgO substrate," *Philos. Mag. Lett.*, vol. 89, no. 8, pp. 493–503, 2009.
[40] J. He et al., "Evolution of nano-fingers in epitaxial Mn-doped Ba (Zr,Ti) O_3 thin films driven by {110} twin boundaries," *Philos. Mag. Lett.*, vol. 91, no. 5, pp. 361–374, 2011.

Jiechao Jiang received the B.Sc. degree in metal physics from the Northeast University, Shenyang, China, in 1987, and the Ph.D. degree in materials physics from the University of Science and Technology Beijing, Beijing, China, in 1993. He held appointments at Stockholm University, Stockholm, Sweden; the University of Marburg, Marburg, Germany; the University of Michigan, Ann Arbor, MI, USA; Louisiana State University, Baton Rough, LA, USA. He is currently a Professor of research with the Department of Materials Science and Engineering and the Facility Manager with the Characterization Center for Materials and Biology, The University of Texas, Arlington, TX, USA. His research interests includematerials characterization using AFM, TEM (analytical, high resolution & in-situ), SEM, XRD, Auger/XPS, and thermal analysis (TGA/DSC), microstructures and defects of advanced functional materials and minerals, atomic structure modeling for new phases, multi-layers and interfaces, nanostructures for nano-electronic and opto-electric devices and nano fuel cells, processing, microstructures, and property relationships in micro/nano-scale materials,nucleation, growth mechanisms, interfaces and surface of epitaxial, and multifunctional coatings.

Nonso Martin Chetuya received the B.Sc. degree in materials science and engineering from the University of North Texas, Denton, TX, USA., in 2016. He is currently working toward the Ph.D. degree in materials science and engineering, focusing on coatings for high-temperature and IR/photonic systems. He is also a Materials Science Engineer specializing in coatings for aerospace systems.

Joseph H. Ngai received the B.Sc. degree in physics from the University of Alberta, Edmonton, AB, Canada, in 2001, the M.Sc. and Ph.D. degrees in physics from the University of Toronto, Toronto, ON, Canada, in 2002 and 2007, respectively. Following postdoctoral training with Yale University, New Haven, 836 CT, USA. He joined the Department of Physics with the University of Texas-Arlington, in 2012, where he is currently an Associate Professor. His research interests include integrating novel materials onto Si using molecular beam epitaxy to expand the functionalities of Si based technologies.

Gordon J. Grzybowski was born in Grand Rapids, MI, USA, in 1980. He received the B.S. degree in chemistry from Central Michigan University, Mount Pleasant, MI, USA, in 2008, and the Ph.D. degree in chemistry from Arizona State University, Tempe, AZ, USA, in 2013. He served in the United States Marine Corps after High School and interned in the materials lab at Smiths Aerospace during his undergraduate studies. Since 2014, he has been a research professional with KBR, Dayton, OH, USA. He is the author of more than 25 articles. His research interests include chemistry of group IV chemical vapor deposition precursors, remote plasma chemical vapor deposition, and group IV alloy photonics.

Efstathios I. Meletis received the Diploma in chemical engineering from the National Technical University of Athens, Athens, Greece, and the M.Sc. and Ph.D. degrees in materials science and engineering (MSE) from the Georgia Institute of Technology (Georgia Tech), Atlanta, GA, USA. He held appointments at Georgia Tech; IIT Research Institute, Chicago, IL, USA; University of California, Davis, Davis, CA, USA; and Louisiana State University, Baton Rouge, LA, USA, where he was an Endowed Professor. He currently is a Distinguished University Professor and the Chair of MSE with The University of Texas at Arlington, Arlington, TX, USA. His research interests include surface engineering, multifunctional thin films, small-scale materials, and material-environment interactions. He has invented novel intensified plasma treatments for surface hardening and producing functionally gradient surface layers. In the area of nanomaterials, his group was the first to achieve self-assembling of perovskite-type oxides and metal/ceramic nanocomposite thin films with high aspect ratio.